



Microstructure and mechanical properties of alloy 617B

Yan GUO, Zhou-bo ZHANG, Rong-can ZHOU, Shu-fang HOU, Bo-han WANG

Xi'an Thermal Power Research Institute Co., Ltd., Xi'an 710032, China

Received 16 May 2014; accepted 11 December 2014

Abstract: The microstructure and mechanical properties of alloy 617B in the process of 5000 h aging at 750 °C were systematically investigated by means of SEM, TEM and mechanical analysis. $M_{23}C_6$ particles were dispersed inside grains and distributed discontinuously along grain boundaries and γ' phases were situated at intragranular sites in the process of aging. The size of precipitates increased with increasing aging time. Inter- and intra-granular carbide and γ' phase particles inside grains resulted in the precipitation strengthening of this aged alloy, enhancing the strength and hardness. The aged alloy possessed good stabilities of hardness and strength during aging. An obvious decrease of the toughness of this aged alloy was due to γ' phase particles limiting plastic deformation to the area nearby grain boundaries, resulting in the occurrence of crack along grain boundaries. Additionally, the intergranular cracks apparently led to a decrease in the toughness for this aged alloy due to carbide particles at grain boundaries. The toughness of this aged alloy was fairly stable possibly due to the unchanged distribution of the precipitates during aging.

Key words: alloy 617B; microstructure; aging; precipitate; hardness; toughness; tensile properties

1 Introduction

The efficient ultra supercritical (USC) power plants, operating at steam temperatures of approximately 600 °C and operating pressures of 25–30 MPa, use high-strength ferritic and austenitic steels (e.g. P92, TP347HFG, Super304, TP310HfNbN) for boiler and turbine components. The urgent need to improve power plant efficiency and thereby reduce CO₂ emission has spurred intensive engineering development of boilers capable of serving at 700 °C or higher temperatures [1,2]. The increased operating parameters place more stringent requirements on the properties of candidate materials and cannot be met by conventional ferritic and austenitic steels. Consequently, there are efforts to replace these materials by Ni-base superalloys due to a combination of excellent microstructural stability, creep-rupture strength, high oxidation and hot corrosion resistance [3,4]. Accordingly, beginning with the European AD700 project in 1998 [5], there has been an extensive international effort to characterize and develop Ni-base superalloys capable of being fabricated and serving

under advanced ultra-supercritical (A-USC) conditions. These superalloys include solid solution strengthened and age-hardened Ni-base alloys such as alloy 617B, Nimonic 263 and Inconel 740H [6–15]. One of the most promising candidate Ni-base superalloys for the boiler superheater tube of 700 °C A-USC units is alloy 617B, which is a modified version of alloy 617 with addition of boron and narrowly tolerated alloying elements, developed by Salzgitter Mannesmann Stainless Tubes, Germany. Alloy 617B has already been tested in 700 °C test loops in Europe [1,2]. The microstructure evolution of alloy 617B during creep was investigated [13]. The present work focuses on the relationship between microstructure and mechanical properties of alloy 617B during aging.

2 Experimental

The chemical composition of alloy 617B investigated in this study is listed in Table 1.

The as-received alloy was solution-treated at 1180 °C for 30 min and water-quenched. It was then aged at 750 °C for 300, 1000, 3000 and 5000 h,

Foundation item: Project (2012AA050501) supported by the National High-tech Research and Development Program of China; Project (NY20110102) supported by the National Energy Applied Technology and Engineering Demonstration Program, China; Project (2012CB724401) supported by the National Basic Research Program of China; Project (003) supported by CSEE Youth Science & Technology Innovation, China

Corresponding author: Yan GUO; Tel: +86-29-82102410; E-mail: gy197704@163.com
DOI: 10.1016/S1003-6326(15)63704-9

Table 1 Chemical composition of alloy 617B (mass fraction, %)

Co	Fe	Ti	Al	B	Cu	W
12.0	0.97	0.41	0.84	0.006	0.02	0.14
Nb	S	P	Sn	C	Si	Mn
0.06	0.0008	0.007	0.0009	0.06	0.15	0.01
Cr	Mo	Pb	Sb	Bi	As	Ni
21.9	8.9	0.0004	0.002	0.0002	0.0008	Bal.

respectively. The hardness of the tested samples was measured with an HB-3000C Brinell hardness tester. The 55 mm × 10 mm × 7.5 mm V-notched Charpy impact sample was tested at room temperature on a PKP450 impact testing machine. Room and high-temperature (700 °C) tensile tests for the tested samples were performed on a CMT5205 tensile testing machine.

For as-received alloys, metallographic samples were ground to 1000-grit and mechanically polished, and then etched using a solution of HCl, HNO₃ and H₂O. For the aged alloys, metallographic samples were ground to 1500-grit and electro-polished with a solution of H₂SO₄ and CH₃OH, then electro-etched with a solution of H₂SO₄ and H₂O. Scanning electron microscope (SEM) investigations were conducted using an FEI Quanta-400HV. Energy dispersive spectroscopy (EDS) micro-analysis was performed by SEM.

Transmission electron microscope (TEM) samples were prepared as follows. A foil of about 500 μm in thickness was cut and mechanically ground to a thickness of 40 μm, from which TEM disks of 3 mm in diameter were punched. Twin-jet electropolishing was performed using a 10% perchloric acid+90% acetic acid solution (volume fraction) at room temperature, with a polishing current of approximately 30 mA. TEM observation was carried out by a JEM-200CX transmission electron microscope (TEM) operating at 200 kV. The phase identification was performed using the selected area electron diffraction (SAED) pattern.

3 Results

The effects of aging time on the room temperature (RT) hardness and impact absorbed energy are presented in Fig. 1. In the as-received condition, the alloy had a low hardness and the highest impact absorbed energy, which is the characteristic for the toughness. A remarkable increase in hardness and an obvious decline in toughness were observed after 300 h aging. After that, the hardness and toughness of the aged alloys were fairly stable and were in the range of HB 207–214 and 66–83 J in the period of 300–5000 h, respectively. The toughness for the aged alloy 617B is higher than that of the aged alloy 740H [16,17].

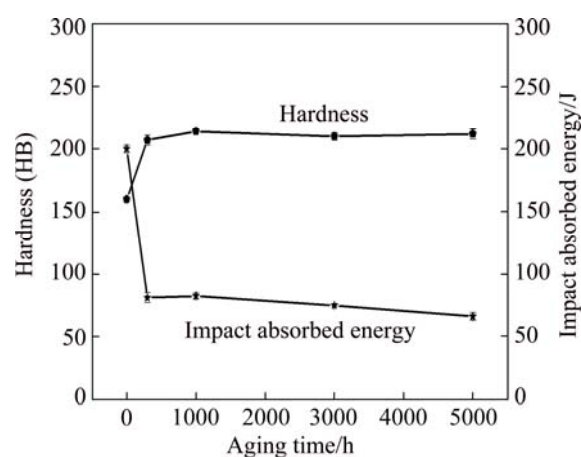
**Fig. 1** Effect of aging time on room temperature hardness and impact absorbed energy of alloy 617B

Figure 2 shows the SEM photographs showing the fractured surfaces after room-temperature impact test of the alloys under different conditions. In the case of the as-received alloy, the fracture surface was predominantly of ductile nature revealed by the occurrence of large equiaxed dimples, presenting a trans-granular pattern, as shown in Fig. 2(a). After aging, the fractographs of the aged alloys indicated a clear brittle fracture with a localized mixed-mode behavior.

The room temperature (RT) tensile properties of the tested alloy are illustrated in Fig. 3. The as-received alloy exhibited low ultimate tensile strength (UTS) and yield strength (YS) and the highest ductility inferred from the highest total elongation (EL). In the period of 300–5000 h, the strength and ductility of the aged alloy fairly maintained stabilities.

The results of tensile tests at 700 °C are depicted in Fig. 4. The as-received alloy exhibited low strength and ductility. After aging, the UTS and YS of the aged alloy increased and remained almost unchanged in the period of 300–5000 h. The ductility of the aged alloy decreased from 75% to 54% with an increase in aging time. In contrast with Fig. 3, it is indicative of a decrease in the strength and an increase in the ductility of the aged alloys at elevated temperature.

Figure 5 shows the microstructural evolution of alloy 617B with aging time. Some large particles (2.4–3.3 μm) distributed within grains were rich in Ti and N, and were therefore probably TiN. High temperature aging led to the precipitation of a large number of particles both within grains and at grain boundaries. The amount of small precipitates increased clearly with prolonging aging time.

Figure 6 presents TEM images and SAED pattern of the alloy aged for 300 h. The sizes of M₂₃C₆ and γ' particles were 25–130 nm and 20–70 nm, respectively (Fig. 6(a)). Figure 6(b) shows the dark-field image of

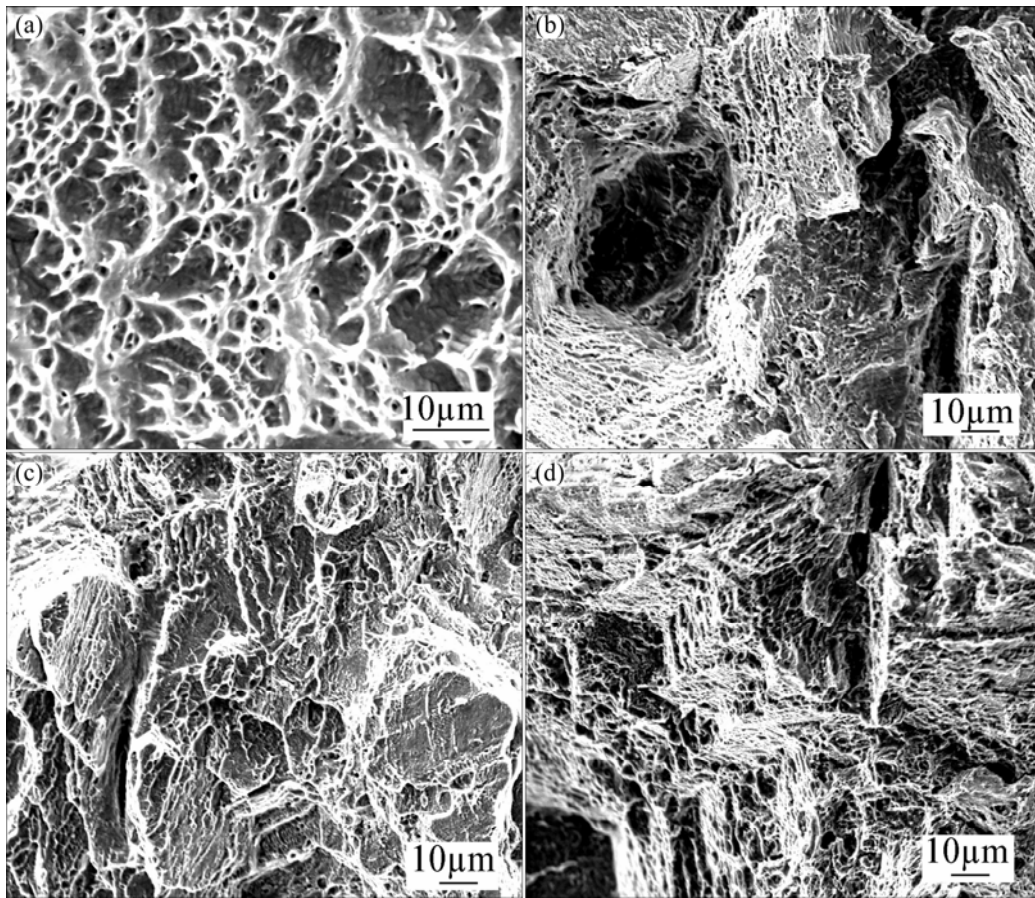


Fig. 2 SEM images revealing effect of aging time on impact fractured surface of alloy 617B: (a) As-received; (b) Aged for 300 h; (c) Aged for 1000 h; (d) Aged for 5000 h

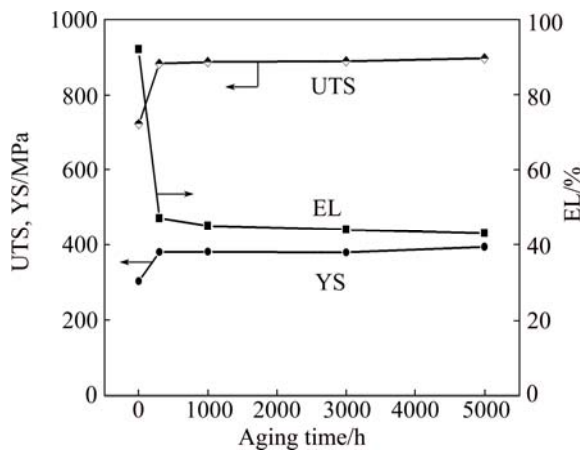


Fig. 3 Effect of aging time on room temperature tensile properties of alloy 617B

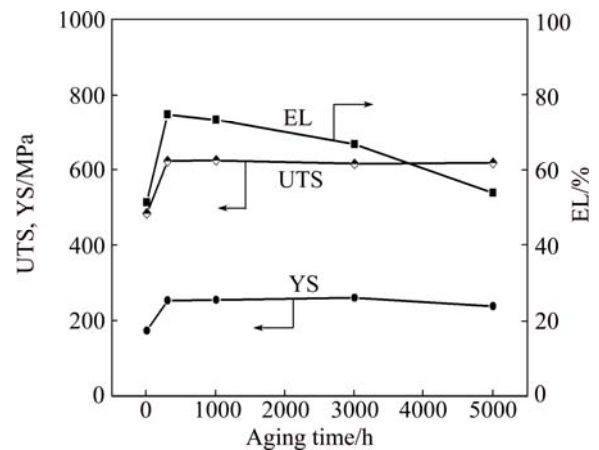


Fig. 4 Effect of aging time on high temperature (700 °C) tensile properties of alloy 617B

$M_{23}C_6$ particles. Figure 6(c) shows the grain size of γ' phase particles distribution evaluated from the TEM micrographs. The average grain size is 39 nm via a size fitting histogram with a Gaussian profile.

TEM morphologies of the precipitates of the alloys aged for 1000 h are presented in Fig. 7. $M_{23}C_6$ particles with a size of 50–150 nm and γ' particles with a diameter of 40–80 nm were observed within grains (Figs. 7(a) and

(b)). $M_{23}C_6$ particle size was estimated to be in range of 100–400 nm at grain boundaries, as shown in Fig. 7(c). The average grain size of γ' phase particles is 54 nm by means of a size fitting histogram with a Gaussian profile (Fig. 7(d)).

Figure 8 reveals the TEM morphologies of the precipitates of the alloys aged for 3000 h. There were $M_{23}C_6$ particles with a size of 50–330 nm and γ' particles

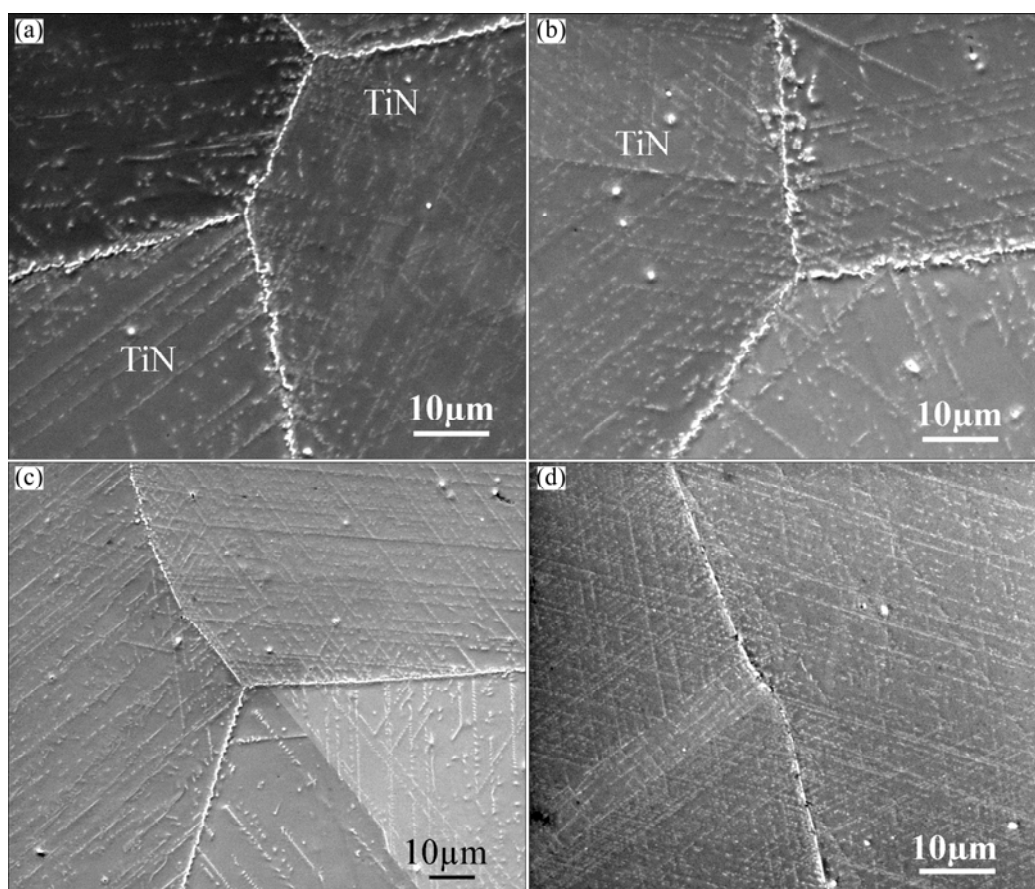


Fig. 5 SEM images of alloy 617B aged for different time: (a) 300 h; (b) 1000 h; (c) 3000 h; (d) 5000 h

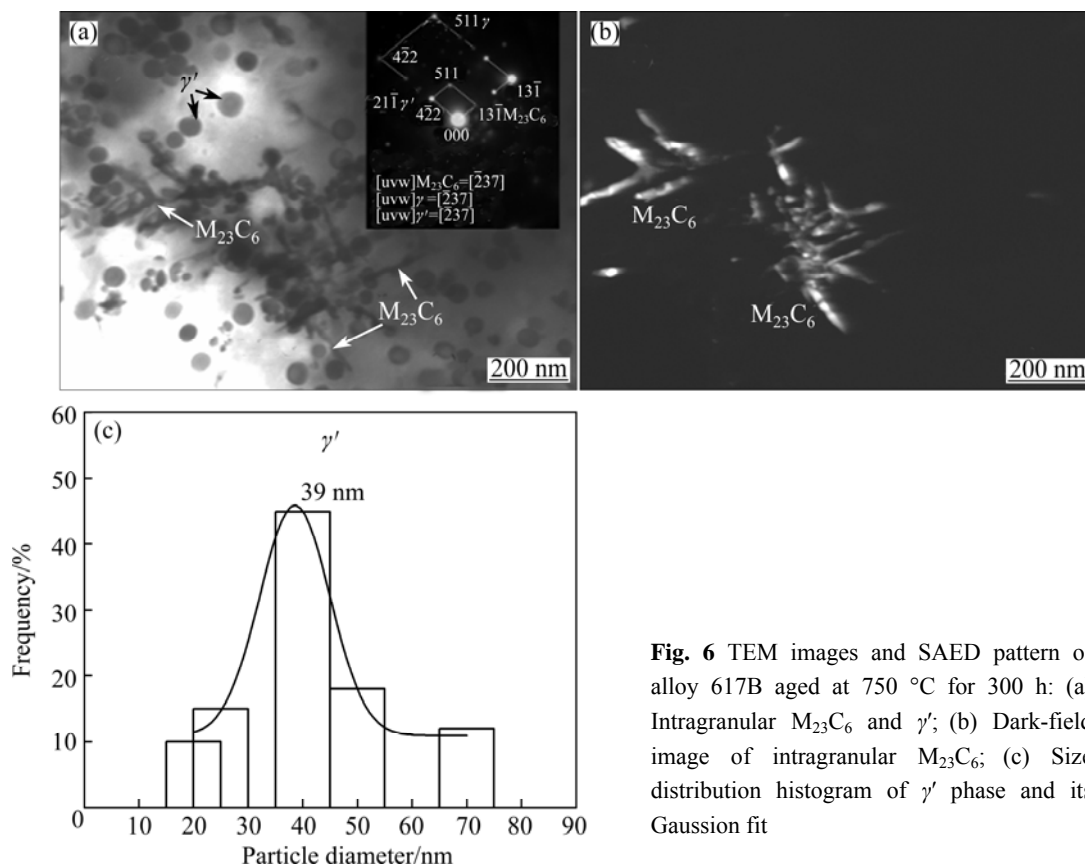


Fig. 6 TEM images and SAED pattern of alloy 617B aged at 750 °C for 300 h: (a) Intragranular $M_{23}C_6$ and γ' ; (b) Dark-field image of intragranular $M_{23}C_6$; (c) Size distribution histogram of γ' phase and its Gaussian fit

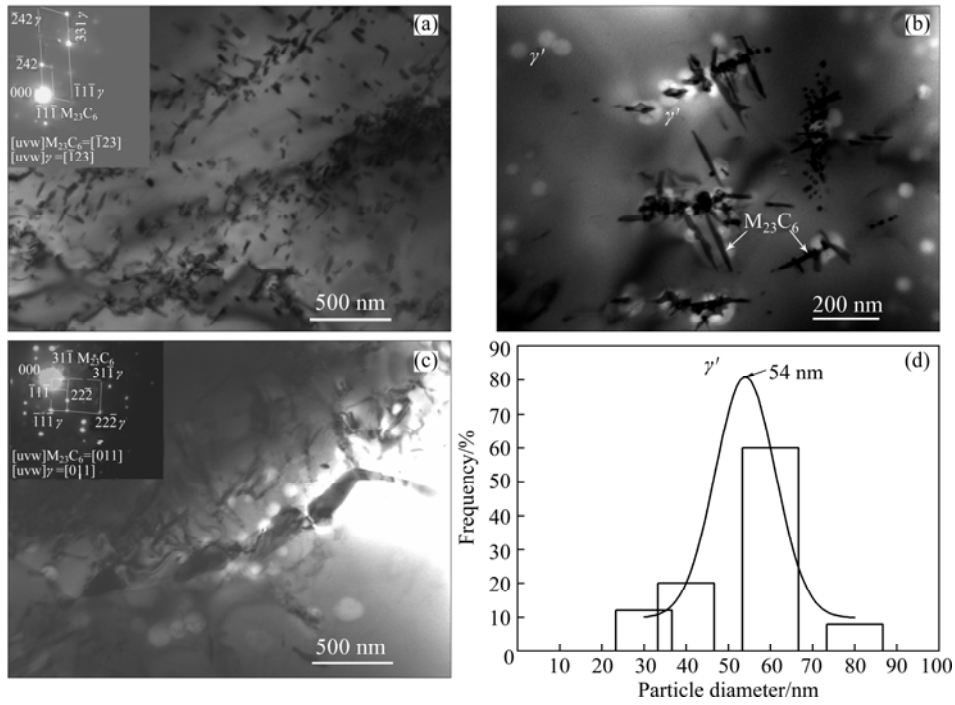


Fig. 7 TEM images and SAED patterns of alloy 617B aged at 750 °C for 1000 h: (a, b) Intragranular $M_{23}C_6$ and γ' ; (c) Discontinuously distributed $M_{23}C_6$ along grain boundaries; (d) Size distribution histogram of γ' phase and its Gaussian fit

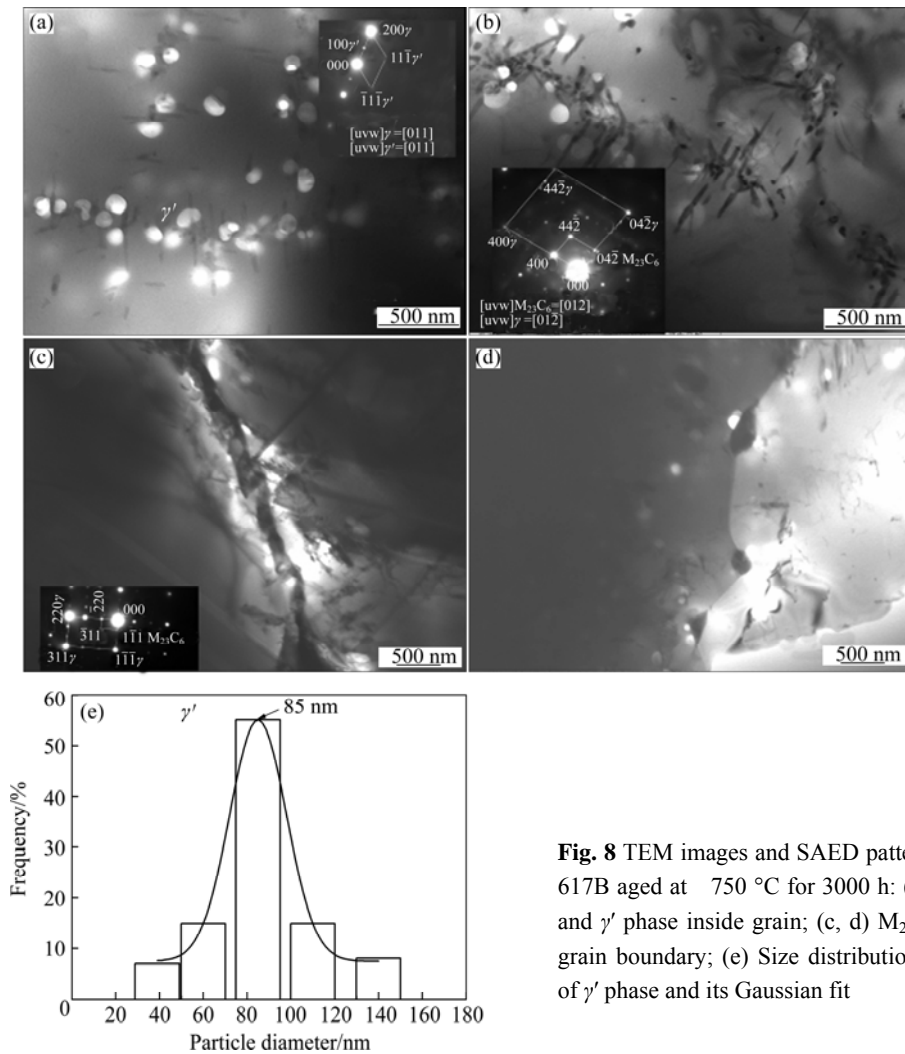


Fig. 8 TEM images and SAED patterns of alloy 617B aged at 750 °C for 3000 h: (a, b) $M_{23}C_6$ and γ' phase inside grain; (c, d) $M_{23}C_6$ phase at grain boundary; (e) Size distribution histogram of γ' phase and its Gaussian fit

with a diameter of 70–130 nm within grains (Figs. 8(a) and (b)). $M_{23}C_6$ particles with a size of 270–500 nm at grain boundaries were observed in Figs. 8(c) and (d). Fitting the particle size of γ' phase particles histogram with a Gaussian profile (Fig. 8(e)) gives an average grain size of 85 nm.

Figure 9 illustrates the size and distribution of the precipitates of the alloys after aging for 5000 h. There were $M_{23}C_6$ particles with a length of 60–300 nm and γ' phase particles with a diameter of 60–170 nm dispersed within grains (Figs. 9(a) and (b)). An average grain size of 91 nm of γ' phase particles is deduced by fitting the particle size histogram with a Gaussian profile (Fig. 9(e)). $M_{23}C_6$ particles with a size of 100–1200 nm discontinuously precipitated along grain boundaries (Figs. 9(c) and (d)). GUO et al [10] reported the carbides particles continuously along grain boundaries for alloy 617 after aging for 5000 h. It is seen from Figs. 6–9 that

the average sizes of γ' particles in alloy aged at 750 °C for 300, 1000, 3000 and 5000 h were about 39, 54, 85 and 91 nm, respectively, which followed the theory of Ostwald ripening [18]:

$$r_t \propto t^{1/3} \quad (1)$$

where r_t is the average radius of γ' phase at time t . The results show that r_t has a linear relationship with $t^{1/3}$, indicating the coarsening behavior of γ' phase followed a diffusion controlled growth procedure.

4 Discussion

From the above results, it was clear that the precipitates of the aged alloy were $M_{23}C_6$ with a complex FCC structure and γ' phase with an ordered FCC structure. $M_{23}C_6$ particles were located both at grain boundaries and inside grains and γ' phase precipitated

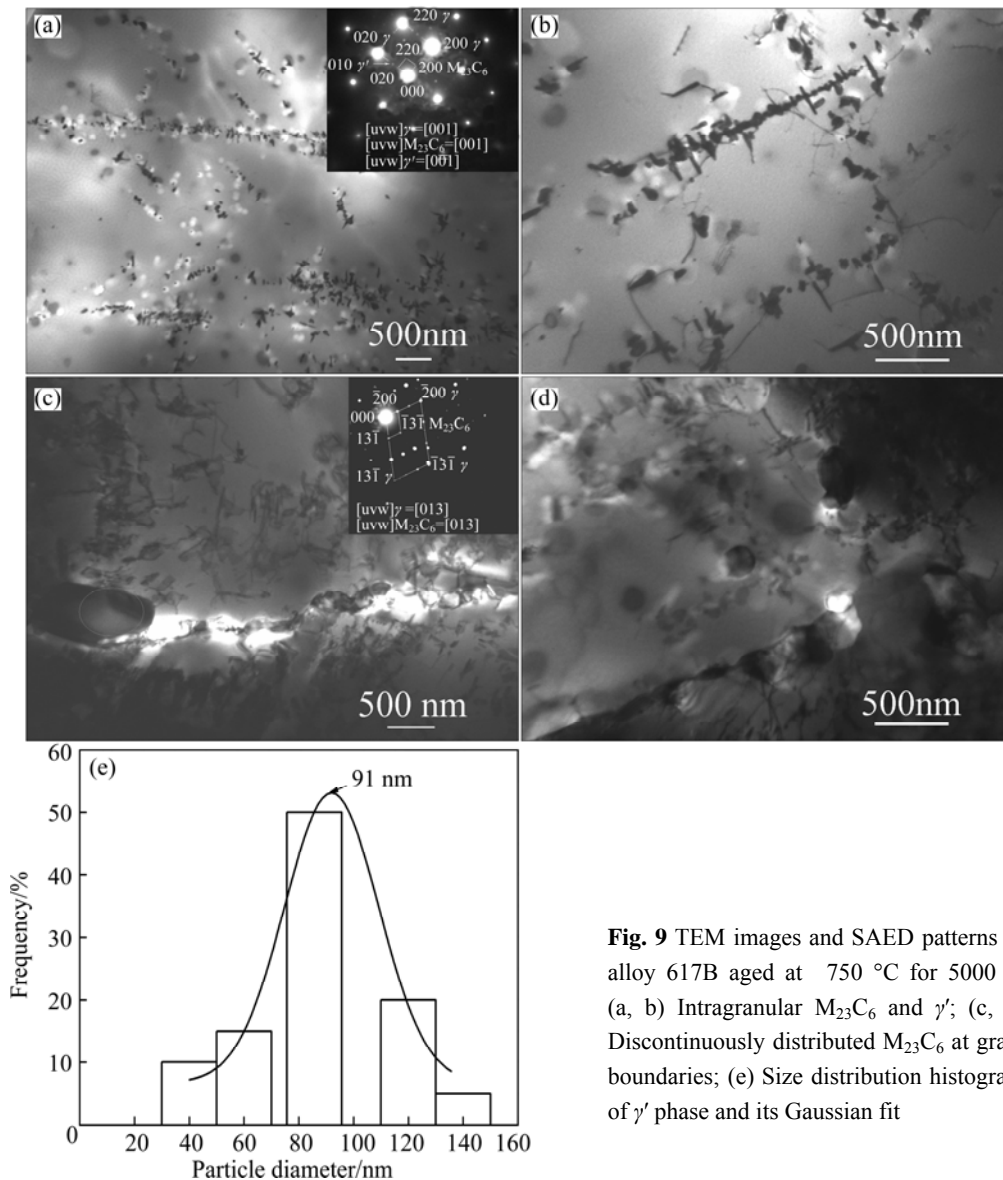


Fig. 9 TEM images and SAED patterns of alloy 617B aged at 750 °C for 5000 h: (a, b) Intragranular $M_{23}C_6$ and γ' ; (c, d) Discontinuously distributed $M_{23}C_6$ at grain boundaries; (e) Size distribution histogram of γ' phase and its Gaussian fit

within grains. Prolonging the aging time resulted in an enhanced amount of the precipitates. It was reported in Ref. [14] that the number of γ' particles in the aged CCA 617 increased greatly after 3000 h aging at 700 and 750 °C; however, γ' particles decreased for the alloy aged at 800 °C for 3000 h. During aging up to 5000 h, the coherency between γ' phase and matrix was remained and the distribution of precipitates at grain boundaries undertook no obvious change. With an increase in aging time, the size of precipitated particles increased. The sizes of intra- and inter-granular precipitates of the alloys aged for different time are summarized in Table 2.

Table 2 Effect of aging time on size of precipitates of alloy 617B aged at 750 °C

Time/h	Size/nm		
	Intragranular γ'	Intragranular $M_{23}C_6$	Intergranular $M_{23}C_6$
300	20–70	25–130	–
1000	30–80	50–150	100–400
3000	70–130	50–330	270–500
5000	60–140	60–300	100–1200

The aged alloy represented enhanced RT hardness and strength compared with as-received samples, which is correlated with the distribution and size of the precipitates and the relationship between the precipitates and the matrix phase. For example, coherency between γ' phase and the matrix was maintained during aging and resulted in a coherent stress for the aged alloy, thus giving rise to enhanced hardness and strength. On the other hand, the strengthening of the aged alloy also results from the precipitation of carbides as discrete particles both inside grains and at grain boundaries. The intragranular carbides contribute to the strengthening effect by acting as barriers for dislocation motion and by stabilizing dislocations. The discrete nature of the grain boundary carbides enhances hardness because it causes pinning of the boundary and decreases grain boundary sliding.

The as-received alloy exhibited the highest RT toughness and ductility revealed by dimple-ductile fracture. A drop in RT toughness and ductility occurred predominately because the carbides formed at grain boundaries after aging. The grain boundaries are weakened by carbides at grain boundary and the separation occurs by decohesion at carbide–matrix interface. At the same time, the interfaces between carbides and the matrix become initiation sites for fracture. Hence, cracks may mainly take place at grain boundaries during the impact and tensile tests. The separated surfaces appear smooth due to the distribution of the grain boundary carbides. These inter-granular

cracks apparently lead to a decrease in RT toughness and ductility for the aged alloys. On the other hand, the precipitation strengthening of γ' phase of the aged alloys limits plastic deformation to the area nearby grain boundaries, resulting in the occurrence of crack along grain boundaries, which is another important factor for a decrease of RT toughness and ductility. The toughness of the aged alloy still maintained a higher level and kept stability because of the unchanged distribution of carbides along grain boundaries in the process of 5000 h aging. It is likely that boron plays an important role in changing the size and distribution of intergranular carbide particles and is conducive to the improvement of bonding at grain boundaries and retards the initiation and propagation of cracks. It was also reported that addition of boron changed the size of intergranular carbides and the fracture mode of steels and alloys [19,20].

5 Conclusions

- 1) The precipitates of the aged alloy are $M_{23}C_6$ carbide located inside grains and at grain boundaries and γ' phase dispersed within grains. The coarsening behavior of γ' followed a diffusion controlled growth procedure.
- 2) During aging, the distribution of the precipitates along grain boundaries takes no obvious change and the coherency between γ' and matrix is maintained. Prolonging aging time induces the growth of precipitates both at grain boundaries and inside grains.
- 3) The aged alloy 617B represents good stabilities of hardness, toughness and tensile strength.

References

- [1] BUGGE J, KJÆR S, BLUM R. High-efficiency coal-fired power plants development and perspectives [J]. *Energy*, 2006, 31(10): 1437–1445.
- [2] ZHAO Shuang-qun, XIE Xi-shan, SMITH GAYLORD D, PATEL SHAILESH J. Research and improvement on structure stability and corrosion resistance of nickel-base superalloy Inconel alloy 740 [J]. *Materials and Design*, 2006, 27(7): 1120–1127.
- [3] LIU Li-rong, JIN Tao, LIU Jin-lai, SUN Xiao-feng, HU Zhuang-qi. Effect of ruthenium on γ' precipitation behavior and evolution in single crystal superalloys [J]. *Transactions of Nonferrous Metals Society of China*, 2013, 23(1): 14–22.
- [4] JAHANGIRI M R, ARABI H, BOUTORABI S M A. Comparison of microstructural stability of IN939 superalloy with two different manufacturing routes during long-time aging [J]. *Transactions of Nonferrous Metals Society of China*, 2014, 24(6): 1717–1729.
- [5] ZHAO Shuang-qun, XIE Xi-shan, SMITH GAYLORD D, PATEL SHAILESH J. The corrosion of INCONEL alloy 740 in simulated environments for pulverized coal-fired boiler [J]. *Materials Chemistry and Physics*, 2005, 90(2–3): 275–281.
- [6] GARIBOLDI E, CABIBBO M, SPIGARELLI S. Investigation on precipitation phenomena of Ni–22Cr–12Co–9Mo alloy aged and

- creep at high temperature [J]. International Journal of Pressure Vessels and Piping, 2008, 85(1–2): 63–71.
- [7] RAHMAN S, PRIYADARSHAN G, RAJA K S, NESBITT C, MISRA M. Investigation of the secondary phases of alloy 617 by scanning Kelvin probe force microscope [J]. Materials Letter, 2008, 62(15): 2263–2266.
- [8] ROSTER J, GOTTING M, del GENOVESE D. Wrought Ni-base superalloys for steam turbine applications beyond 700 °C [J]. Advanced Engineering Materials, 2003, 5(7): 469–483.
- [9] WU Q, SONG H, ROBERT W, SHINGLEDECKER J P, VASUDEVAN V K. Microstructure of long-term aged IN617 Ni-base superalloy [J]. Metallurgical and Materials Transactions A, 2008, 39(11): 2569–2585.
- [10] GUO Y, WANG B H, HOU S F. Aging precipitation behavior and mechanical properties of Inconel 617 superalloy [J]. Acta Metallurgica Sinica, 2013, 26(4): 307–312.
- [11] ROSTER J, GOTTING M, del GENOVESE D, BÖTTGER B, KOPPEL R, WOLSKE M, SCHUBERT F, PENKALLA H J, SELIGAT, THOMA A, SCHOLZ A, BERGER C. Wrought Ni-base superalloys for steam turbine applications beyond 700 °C [J]. Advanced Engineering Materials, 2003, 5(7): 469–483.
- [12] SAUDERS J, MONTERIRO M, RIZZO F. The oxidation behavior of metals and alloys at high temperatures in atmospheres containing water vapor: A review [J]. Progress in Materials Science, 2008, 53(5): 775–837.
- [13] EVANS N D, MAZIASZ P J, SWINDEMAN R W, SMITH G D. Microstructure and phase stability in INCONEL alloy 740 during creep [J]. Scripta Materialia, 2004, 51(6): 503–507.
- [14] ZHAO S Q, JIANG Y, DONG J X, XIE X S. Experimental investigation and thermodynamic calculation on phase precipitation of INCONEL 740 [J]. Acta Metallurgica Sinica, 2006, 19(6): 425–431.
- [15] GUO Y, ZHOU R C, HOU S F, ZHANG H J. Analysis of microstructure and mechanical properties of alloy 617 aged at 760 °C [J]. Proceedings of the CSEE, 2010, 30(26): 86–89.
- [16] XIE X S, ZHAO S Q, DONG J X, ZHANG M C. Structural stability and improvement of Inconel alloy 740 for ultra supercritical power plants [J]. Journal of Chinese Society of Power Engineering, 2011, 31(8): 638–641. (in Chinese)
- [17] CHI Cheng-yu, YU Hong-yao, XIE Xi-shan. Critical high temperature materials for 700 °C A-USC power plants [J]. World Iron & Steel, 2013, 2: 42–57.
- [18] ZHAO S Q, XIE X S, GAYLORD D, SMITH S, PATEL J. Microstructure stability and mechanical properties of a new nickel-base superalloy [J]. Materials Science and Engineering A, 2003, 355(1–2): 96–105.
- [19] MUKHERJI D, RÖSLER J, KRÜGER M, HEILMAIER M, BÖLITZ M C, VÖLKL R, GLATZEL U, SZENTMIKLÓSI L. The effects of boron addition on the microstructure and mechanical properties of Co–Re-based high-temperature alloys [J]. Scripta Materialia, 2012, 66(1): 60–65.
- [20] ABE F, TABUCHI M, TSUKAMOTO S. Mechanisms for boron effect on microstructure and creep strength of ferritic power plant steels [J]. Energy Materials, 2012, 4(4): 166–174.

镍基合金 617B 的微观组织与力学性能

郭岩, 张周博, 周荣灿, 侯淑芳, 王博涵

西安热工研究院有限公司, 西安 710032

摘要: 采用 SEM、TEM 和力学性能测试研究镍基合金 617B 在 750 °C 下时效 5000 h 过程中的微观组织稳定性和力学性能。在时效过程中, 合金 617B 析出 $M_{23}C_6$ 碳化物和 γ' 相, 前者分布于晶界和晶内, 后者分布于晶内。随着时效时间的延长, 析出物颗粒尺寸逐渐增大。碳化物和 γ' 相颗粒起到析出强化作用, 并提高时效态合金的硬度和强度。在时效过程中, 时效态合金的强度和硬度具有良好的稳定性。合金 617B 时效后的韧性降低是由于 γ' 相抑制晶界附近的弹性变形, 导致晶界裂纹形成; 此外, 晶界碳化物析出导致其与基体相的界面强度降低, 晶界处易产生裂纹。这使得时效态合金的冲击韧性降低。但在时效过程中, 时效态合金的韧性具有较好的稳定性是由于时效 5000 h 过程中析出相的分布未发生明显变化。

关键词: 617B 镍基合金; 微观组织; 时效; 析出; 硬度; 韧性; 拉伸性能

(Edited by Xiang-qun LI)